Electronic Supplementary Material (ESI) for Analyst.
This journal is © The Royal Society of Chemistry 2021

Enhanced crystallisation kinetics of edible lipids through the action of a bifurcated streamer

Jack J. Youngs[a], Peter R. Birkin[a], Juhee Lee[c], Tadd T. Truscott[b] and Silvana Martini[c]

[a] Department of Chemistry, University of Southampton, Southampton, UK, SO17 1BJ

[b] Department of Mechanical and Aerospace Engineering, Utah State University, Logan, UT, 84322-4130, USA

[c] Department of Nutrition, Dietetics, and Food Sciences, Utah State University, Logan, UT, 84322-8700, USA

Supplementary Material

The apparatus set-up utilised for all lipid crystallisation experiments is depicted in Figure 1 in the main text. All-purpose shortening (APS) sample initially agitated, on a laboratory stirrer plate at 200 rpm with stirrer bar (S), within a thermostabilised cell to cool sample to the desired crystallisation temperature. Piston-like emitter (PLE) ultrasound source (20 kHz) was positioned approximately central within the cell, with a hydrophone (H) device positioned to one side. Ultrasound was applied in the presence of pre-existing lipid crystals. This produces a bubble population consisting of a cavitation cluster in addition to gas bubbles located in the bulk oil.

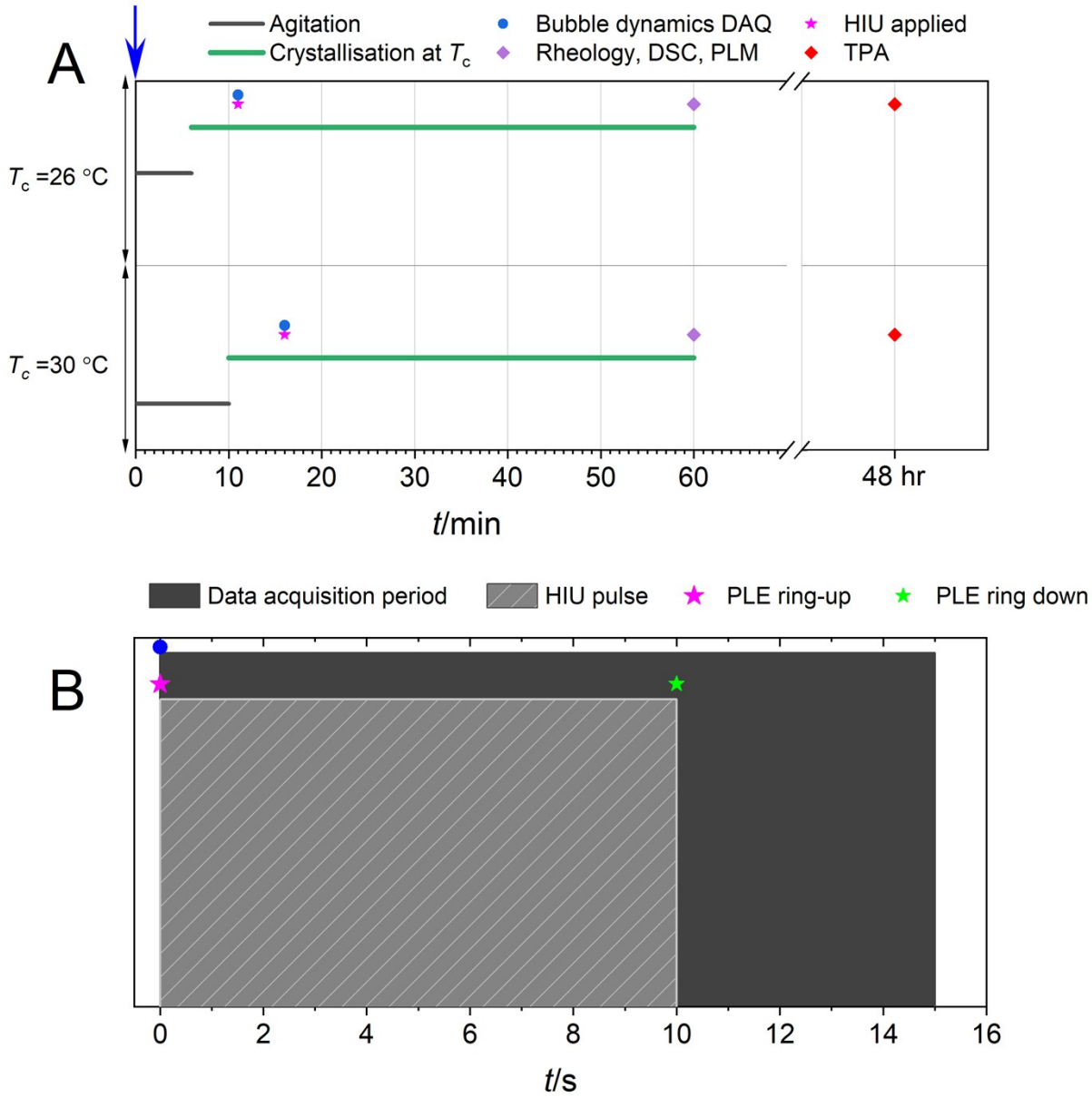

Figure S1. (**A**)Timeline for isothermal crystallisation of APS at T_c = 26 and 30 °C. The transfer of APS to crystallisation cell and start of SFC measurements (recorded every 30 s for total 60 minute period) (↓), initial agitation period (—), crystallisation of oil sample at selected T_c (▬), application of HIU (🡅) and physicochemical analyses (◆ and ◆) are indicated. (**B**) Time period of data acquisition (DAQ) of bubble dynamics present (●) is

highlighted. HIU applied as a 10 s pulse (▨) within a 15 s DAQ time window (○), with the PLE ring-up (↑) and following ring-down (↑) processes present.

The timeline for isothermal crystallisation of APS sample is detailed in Figure S1 (A). Key time markers for HIU application, measurement of SFC, bubble dynamics and physicochemical analysis are highlighted. Figure S1 (B) illustrates the data acquisition window for bubble dynamics, recording hydrophone data during the 10 s HIU pulse, in addition to a further 5 s after which HIU is terminated. The time point of PLE ring up and PLE ring down processes are highlighted.

Figure S2 shows the viscous modulus (*G''*) recorded within the APS lipid samples, with and without the application of high-intensity ultrasound. At T_c = 26 °C samples crystallised in the presence of HIU were significantly greater than the woHIU treatment for HIU powers greater or equal to 51 W. In contrast, samples treated with HIU at power levels greater or equal to 18 W showed significantly larger mean *G''* values compared to untreated samples.

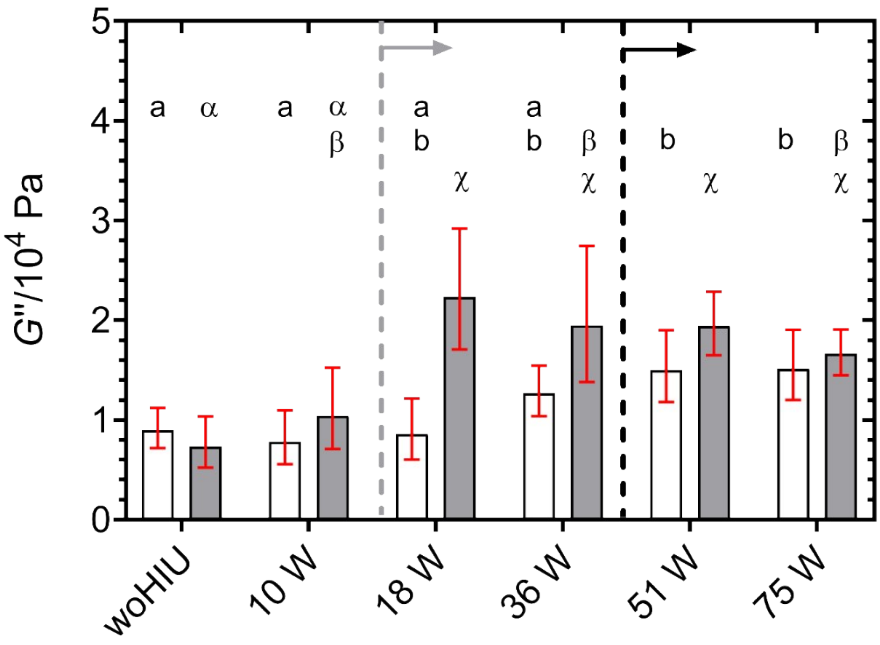

Figure S2. Viscous modulus of an all-purpose shortening sample crystallised at 26 °C (●) and 30 °C (○) in the presence and absence (woHIU) of high intensity ultrasound applied at power levels of 10 W, 18 W, 36 W, 51 W and 75 W. Mean values are reported with 95 % confidence levels. Individual *G*" values become significantly different from the woHIU treatment at T_c = 26 °C (black dash ▬ ▬) and 30 °C (grey dash ▬ ▬) as indicated.

The strain (%) at the crossover point between the elastic (*G*') and viscous (*G*") moduli curves can be determined for each of the HIU treatments and supercooling conditions, as illustrated in Figure S3.

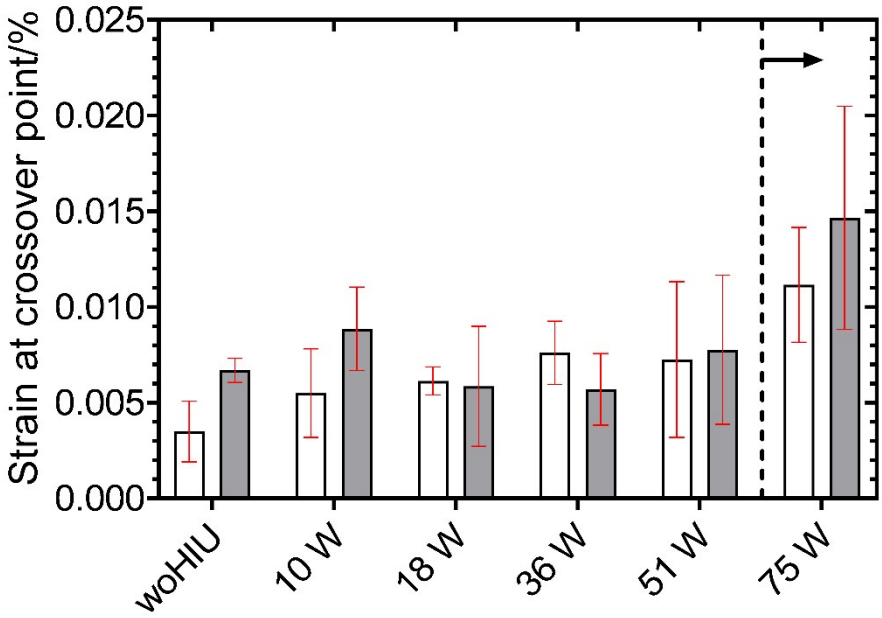

Figure S3. Strain at crossover point (where *G*'=*G*'') for an all-purpose shortening sample crystallised at T_c = 26 °C (●) and 30 °C (○) in the presence and absence (woHIU) of high intensity ultrasound applied at power levels of (10, 18, 36 , 51 and 75) W. Mean values are reported with 95 % confidence levels. Individual strain values become significantly different from the woHIU treatment at both supercooling temperatures as indicated (black dash ▬ ▬).

The physicochemical properties were recorded for an APS lipid sample in the absence and presence of HIU, delivered at selected power levels between (10-75) W. Two crystallisation temperatures (T_c = 26 °C (❋) and 30 °C(◆)) were investigated. In each case, the changes relative to the without HIU treatment were determined and results are illustrated within Figure S4. Values were also normalised to the delivered HIU power, to elucidate the energy efficiency of the HIU treatment conditions. Changes in the sample hardness (ΔHA) relative to the woHIU treatment are given in Figure S4 (**A**) and the changes per watt of power (ΔHA_E) are detailed within Figure S4 (**B**).

The change in sample hardness showed little difference between 26 °C and 30 °C temperatures over the HIU power level range. In addition, the greatest change per watt was seen for 10 W HIU treatment at 30 °C, however, this was insignificant compared with higher ultrasonic powers. Whereas the presence of the BiS environment (10 W) had a very weak effect upon the sample hardness at 26 °C, relative to greater HIU power levels.

In addition, changes in viscous modulus ($\Delta G''$) (**C**) and changes per watt ($\Delta G''_E$) (**D**). Values of ΔG'' were independent of crystallisation temperature for all HIU power levels except 18 W, which showed the greatest energy efficiency ($\Delta G''_E$) relative to the woHIU case. In contrast, values for $\Delta G''_E$ were insignificant at 26 °C.

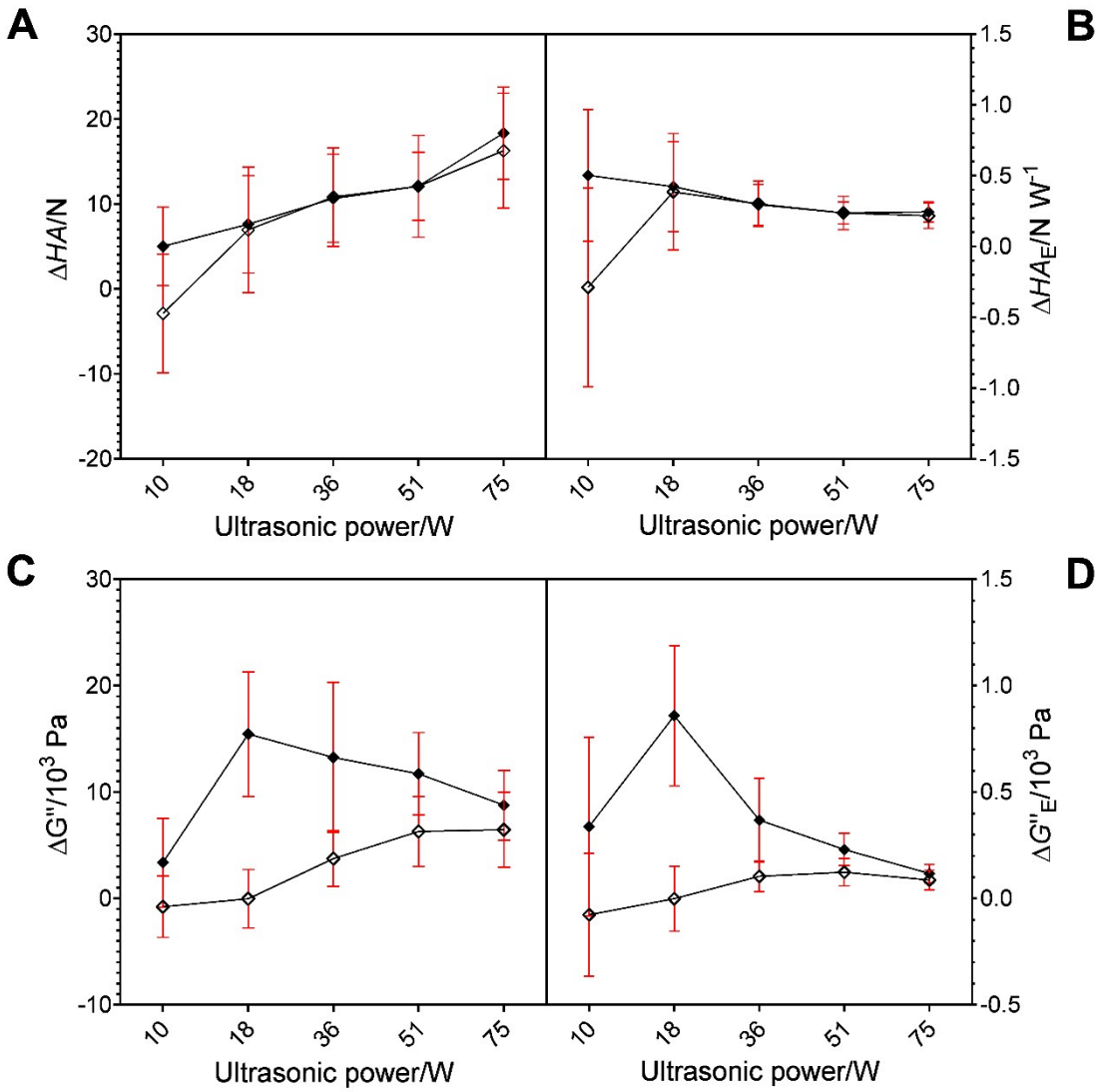

Figure S4. Change in physicochemical properties from the isothermal crystallisation of all-purpose shortening in the presence of HIU, delivered at selected powers between 10-75 W with respect to untreated (woHIU) samples, at T_c = 26 °C (✱) and 30 °C(◆). Change in sample hardness (ΔHA) (**A**) and change per W (ΔHA_E) (**B**), change in viscous modulus ($\Delta G''$) (**C**) and change per W ($\Delta G''_E$) (**D**). Mean values are plotted with 95% CL.

The raw values (mean ± 95 % CL) are tabulated below for T_{sc} = 26 °C and 30 °C (Table S4) in the presence of each HIU treatment.

The melting profiles of an APS sample crystallised in the absence and the presence of HIU delivered at selected powers between (10-75) W at T_c = 26 °C and 30 °C are given in Figure S5 below.

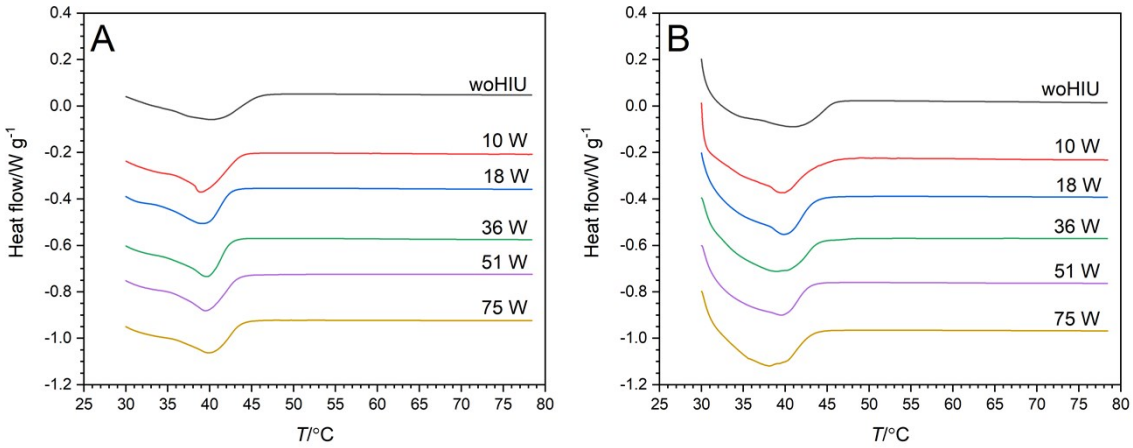

Figure S5. DSC melting profiles of APS crystallised for 60 min at T_c = 26 °C (**A**) and 30 °C (**B**) with and without HIU, delivered at powers of (10, 18, 36, 51 and 75) W using 20 kHz frequency.

Solid fat content *vs.* time curves, recorded for crystallisation within an all-purpose shortening (APS) sample, were fitted to the Gompertz model. This was conducted in the absence and presence of high-intensity ultrasound, delivered at selected powers between (10-75) W at T_c = 26 °C and 30 °C. The changes in the fitting parameters, relative to the woHIU case (mean ± 95 % CL) are summarised below (Table S1).

Table S1 displays the change in induction time relative to the woHIU treatment ($\Delta\lambda$) and the change per watt of applied power ($\Delta\lambda_E$) alongside the change in maximal growth rate with respect to without HIU treatment ($\Delta\mu$) and the change per watt of power ($\Delta\underline{\mu}_E$).

	HIU	$\Delta\lambda$/min	$\Delta\lambda_E$/min W^{-1}	HIU	$\Delta\mu$/% min^{-1}	$\Delta\mu_E$/% min^{-1} W^{-1}
T_c = 26 °C	10 W	-2 ± 1^{a}	-0.2 ± 0.2^{a}	10 W	0.5 ± 0.3^{a}	0.05 ± 0.03^{a}
	18 W	-4 ± 1^{a}	-0.24 ± 0.08^{a}	18 W	0.7 ± 0.2^{a}	0.037 ± 0.009^{a}
	36 W	-4 ± 1^{a}	-0.11 ± 0.04^{a}	36 W	0.8 ± 0.4^{a}	$0.02 \pm 0.01^{a,b}$
	51 W	-5 ± 1^{a}	-0.09 ± 0.03^{a}	51 W	0.7 ± 0.2^{a}	0.014 ± 0.004^{b}
	75 W	-4 ± 1^{a}	-0.06 ± 0.02^{a}	75 W	0.8 ± 0.1^{a}	0.011 ± 0.002^{b}
T_c = 30 °C	10 W	$-9 \pm 1^{\alpha}$	$-0.9 \pm 0.2^{\alpha}$	10 W	$0.4 \pm 0.1^{\alpha}$	$0.04 \pm 0.01^{\alpha}$
	18 W	$-5 \pm 1^{\beta}$	$-0.28 \pm 0.08^{\beta}$	18 W	$0.14 \pm 0.04^{\alpha}$	$0.008 \pm 0.002^{\beta}$
	36 W	$-9 \pm 1^{\alpha,\chi}$	$-0.26 \pm 0.05^{\beta}$	36 W	$0.20 \pm 0.07^{\alpha}$	$0.006 \pm 0.002^{\beta}$
	51 W	$-12 \pm 1^{\chi,\delta}$	$-0.25 \pm 0.03^{\beta}$	51 W	$0.25 \pm 0.05^{\alpha}$	$0.005 \pm 0.001^{\beta}$
	75 W	$-14 \pm 1^{\delta}$	$-0.19 \pm 0.02^{\beta}$	75 W	$0.35 \pm 0.04^{\alpha}$	$0.005 \pm 0.001^{\beta}$

Table S1. Change in induction time ($\Delta\lambda$) with respect to without HIU treatment and the change per watt of power ($\Delta\lambda_E$) recorded from isothermal crystallisation of all-purpose shortening sample with HIU delivered at selected power levels between (10-75) W. Change in growth rate ($\Delta\mu$) with respect to without HIU treatment and change per watt of power ($\Delta\mu_E$). Values calculated from Gompertz curve fitting. Values given for each HIU treatment (mean ± 95% CL), at 26 °C and 30 °C. Values with the same superscript are not significantly different ($p < 0.0001$).

ΔT_{sc}/ °C	Ultrasonic power/W	T_p/°C	ΔH_m/J g^{-1}
9	woHIU	40.0 ± 0.4^{a,b}	14.7 ± 0.8^{a}
	10	39.1 ± 0.6^{a}	15 ± 2^{a}
	18	39.5 ± 0.6^{a,b}	15.5 ± 0.8^{a}
	36	39.7 ± 0.5^{a,b}	15 ± 1^{a}
	51	39.8 ± 0.6^{a,b}	15 ± 1^{a}
	75	40.1 ± 0.4^{b}	15 ± 1^{a}
ΔT_{sc}/ °C	Ultrasonic power/W	T_p/°C	ΔH_m/J g^{-1}
5	woHIU	40.9 ± 0.2$^{\alpha}$	11.1 ± 0.4$^{\alpha}$
	10	40.0 ± 0.5$^{\beta}$	12 ± 1$^{\alpha,\beta}$
	18	39.8 ± 0.3$^{\beta}$	13 ± 1 $^{\alpha,\beta}$
	36	39.5 ± 0.7$^{\beta}$	12.7 ± 0.3 $^{\alpha,\beta}$
	51	40.0 ± 0.3$^{\beta}$	13.5 ± 0.6$^{\beta}$
	75	39.8 ± 0.5$^{\beta}$	14.0 ± 0.7$^{\beta}$

Table S2. Peak melting temperature (T_p) and enthalpy of melting (ΔH_m) values (mean ± 95 % CL) for all-purpose shortening sample crystallised in the absence (woHIU) and presence of HIU, delivered at selected HIU powers between (10-75) W, at two crystallisation temperatures (ΔT_{sc} = 9 °C and 5 °C). Values with different superscripts are significantly different ($p < 0.005$)

The decay within the hydrophone envelope over the 10 second pulse can be fitted to an empirical model based on a second order approach. This was conducted for each of the HIU treatment conditions, and the hydrophone data was first normalised to the maximum signal voltage. The effective second order constant (k) for each treatment is summarised in Table S3. It should be stressed that this model is empirical at this time and further theory and experiment is needed to quantify this process fully.

ΔT_{sc}/ °C	Ultrasonic power/W	Second order rate constant, k/ V^{-1} s^{-1}	r^2
9	10	$0.07 \pm 0.06^{a,b}$	0.700
	18	0.05 ± 0.01^{b}	0.935
	36	$0.32 \pm 0.02^{c,d}$	0.953
	51	0.35 ± 0.04^{d}	0.939
	75	0.58 ± 0.04^{e}	0.922
ΔT_{c}/ °C	Ultrasonic power/W	k/ V^{-1} s^{-1}	r^2
5	10	$0.01 \pm 0.05^{\alpha}$	0.290
	18	$0.02 \pm 0.04^{\alpha}$	0.688
	36	$0.12 \pm 0.02^{\alpha}$	0.944
	51	$0.25 \pm 0.03^{\beta}$	0.908
	75	$0.28 \pm 0.01^{\beta}$	0.970

Table S3. Rate constant (k) obtained from a second order kinetics model corresponding to the decay in the average hydrophone signal as high-intensity ultrasound (HIU) is applied over a 10 s period. Fitting was conducted for HIU power levels of 10 W, 18 W, 36 W, 51 W and 75 W for ΔT_{sc} = 9 °C and 5 °C. Values with the same superscripts are not statistically different ($p < 0.0001$) (mean ± 95 %CL)

The acoustic emission within sonicated all-purpose shortening samples was characterised using hydrophone pressure measurements over the 10 s HIU pulse duration. This was conducted at T_c = 30 °C and in the presence of each unique bubble cluster event between ultrasonic powers of (10-75) W, as given by Figure S6 below.

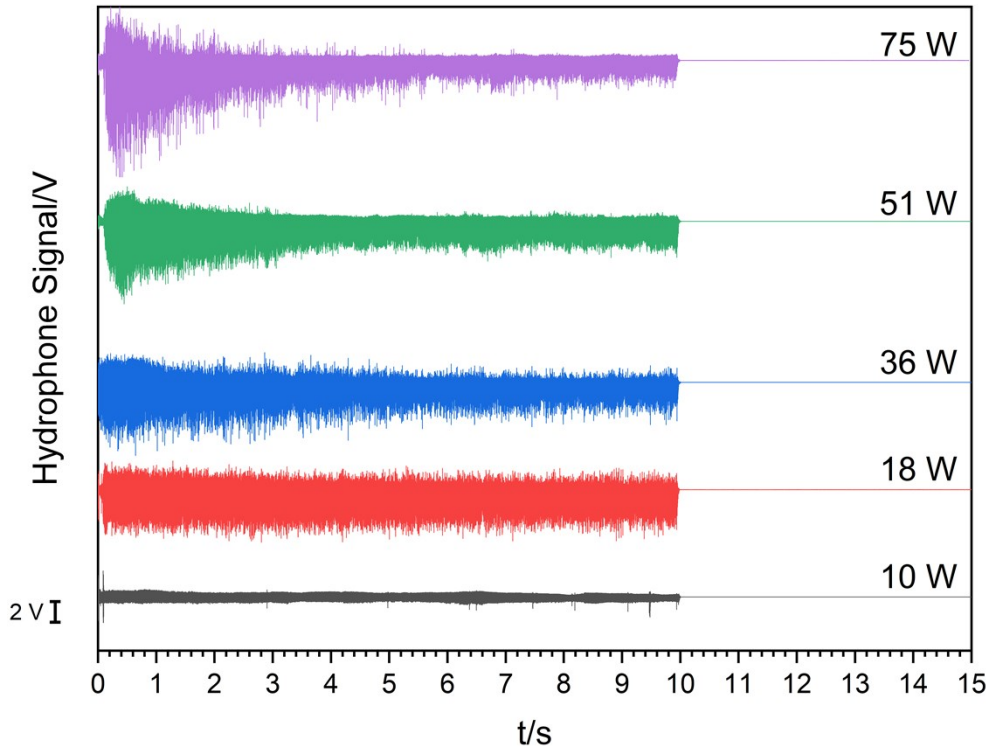

Figure S6. Hydrophone time series collected during HIU treatment in APS (T_c = 30 °C) for 10 s pulse duration and a further 5 s after the cavitation period. HIU powers are indicated by each trace. Scale bar represents 2 V for hydrophone signal for comparison.